Composite Structures 337 (2024) 118056

Contents lists available at ScienceDirect

Composite Structures

journal homepage: www.elsevier.com/locate/compstruct

Thermoplastic composite injection-overmoulding with indirectly-loaded reinforcement: Design for manufacture

A.J. Parsons [a,*], S. Chen [a,1], A. Ryder [b], D. Bradley [c], N.A. Warrior [a], L.T. Harper [a]

[a] Composites Research Group, Faculty of Engineering, University of Nottingham, NG7 2RD, UK
[b] Surface Generation Ltd., Leicester LE15 8TW, UK
[c] IACMI Scale-up Research Facility, Michigan State University, Detroit, MI, USA

ARTICLE INFO

Keywords:
Finite element analysis
Composite overmoulding
Manufacturing
Thermoplastic
Interface
Joint

ABSTRACT

Thermoplastic Overmoulding is an emerging manufacturing method combining low-cost, high-rate injection moulding with continuous fibre composite elements. The combination of materials with dissimilar stiffnesses can create stress concentrations and warpage, with further complications caused by high injection pressures distorting the continuous fibre elements (wash). This study uses a numerical model to consider a particular overmoulding approach that utilises a strategically positioned local reinforcing element (an insert) that is loaded indirectly via stresses transferred from the surrounding overmoulding material. This offers a low-cost solution by minimising use of continuous fibre material, but has a higher likelihood of the aforementioned problems. A geometrical solution (a waffle-type structure) is used to address these manufacturing challenges without compromising the primary stiffening role of the continuous fibre element. An insert efficiency factor is proposed to describe the tensile behaviour and the diminishing returns on peak load in the insert when embedding increasingly higher stiffness inserts into moderate stiffness overmoulding materials containing short fibres. According to the simulation results, the proposed Waffle structure should provide stiffness commensurate with the conventional configuration; however, the experimental coupons highlight the complexities of injection moulding short fibres and indicate the detrimental effect of anisotropic fibre distributions within the overmoulded sections.

1. Introduction

Injection overmoulding of fibre reinforced thermoplastics is a relatively new field, emerging in the mid-2000s to explore structural applications within the automotive and aerospace sectors. Typically, low-cost, fibre-filled injection moulding polymers are combined with high stiffness, high strength continuous fibre organosheets. In this way, manufacturing can be simplified such that the continuous fibre material requires only a moderate change in shape during forming, while the discontinuous material is used to generate complex geometrical features via injection moulding. The resulting process is rapid, with Takt times similar to conventional injection moulding (typically less than 2 min). The overall part cost is minimised by only using high-performance materials in areas where they are truly required to satisfy the loading conditions.

Injection overmoulding can be broadly split into two categories: 1-stage and 2-stage. In 1-stage overmoulding the continuous fibre element is heated and formed in the same matched tool as the injection moulding. In 2-stage, the continuous fibre element is pre-shaped and then introduced to the mould for overmoulding as a separate operation. Each process has limitations that need to be overcome. The 1-stage process typically achieves a better interfacial bond strength between the continuous and discontinuous fibre phases, due to high interface temperatures that can provide rapid molecular diffusion and healing [1–5], but the continuous fibre element is highly susceptible to deformation. In the 2-stage process the reverse is true – the continuous element is more stable, but the interface bonding is less developed. Gaps or micro-cracking can occur at the edges of reinforcing elements during 2-stage overmoulding, due to freezing before full consolidation, resulting in poor interfacial strength [4,6–8]. Considerable deflections of the continuous element have also been observed during 1-stage overmoulding that benefit interface strength due to improved mechanical interlocking, but at a cost to in-plane properties [4,9,10]. Tanaka et al. [11–16] provided a series of reports considering how to manage this

* Corresponding author.
E-mail address: andrew.parsons@nottingham.ac.uk (A.J. Parsons).
[1] Present address: School of Mechanical Engineering, Xi'an Jiaotong University, Xi'an 710049, People's Republic of China.

https://doi.org/10.1016/j.compstruct.2024.118056
Received 11 August 2023; Received in revised form 18 January 2024; Accepted 21 March 2024
Available online 22 March 2024

deformation. It is apparent that the quality of the interface is a key factor in successful overmoulding and that it is significantly affected by the manufacturing process. Poor bonding at the overmoulding interface can typically create the weakest point of the structure and can lead to significant weight penalties if not designed out correctly. The manufacturing strategy is therefore critical to the success of the final component.

The majority of applications using injection overmoulding to date have been concerned with adding discontinuous fibre-filled local stiffening features, such as ribs, to otherwise continuous fibre reinforced surfaces with gentle curvature [17]. The primary loads are directly carried through the continuous fibre skin, which also defines the boundary of the part. This provides a structural component and this approach has seen considerable research interest for mainly aerospace applications, since the component cost is dominated by the volume of the continuous fibre organosheet.

Composite overmoulding is also in development for applications within the automotive industry [18,19], where the primary drivers are cost and stiffness. Components for these applications tend to be created with smaller discrete continuous fibre elements, or 'inserts'. These inserts are loaded indirectly, i.e. the load pathway extends beyond their edges, with the intention to introduce a local stiffening effect to the otherwise randomly orientated short fibre-filled polymer. Such an arrangement has several design and manufacturing challenges. In terms of design, while stiffness can be increased, an abrupt transition from the insert to the overmoulding material results in stress concentrations at the interface and a reduction in overall strength. This stress concentration is due to the mismatch in stiffness between the two materials, therefore the stress efficiency of the insert (ratio of the peak stress carried by the insert during component loading compared to the failure stress of the insert) is low. This transition must be managed through a combination of laminate design rules and geometrical solutions in order to minimise knockdown in strength. One such solution is investigated in this study.

Discrete inserts also exacerbate potential manufacturing problems, such as warpage and fibre wash [20]. Conventionally, an insert would be positioned at one face of an injection mould tool during manufacturing, as it is easier to clamp the insert in place and directly transfer heat through conduction. The position of the insert also provides preferential stiffening in bending, as it is positioned further away from the neutral axis. Within the context of this paper, such a configuration will be referred to as 'Bias' positioning. Whilst there are benefits to this approach, there are also significant drawbacks however, notably difficulties maintaining a desired part geometry due to differential shrinkage behaviour between the insert and the overmoulding material. This can lead to considerable residual stress and therefore warping of the part (see Fig. 1), negatively impacting mechanical performance.

There is also a need to restrain the insert in place during injection moulding to prevent fibre washing. To achieve this, the tool is designed to clamp the insert using 'pinch points', resulting in recessed areas that are not filled with overmoulding material. These must be carefully considered to avoid generating weak areas, while also providing sufficient clamping force to prevent surface wash. Surface wash can occur when the unsupported edge of an insert is exposed to the flow front of the injected material (see Fig. 2).

This paper focuses on overmoulding using indirectly loaded insert reinforcements, produced using the 2-step injection process. It explores potential solutions to mitigate the manufacturing issues of warpage and fibre wash in a simple panel containing a discrete reinforcing insert, whilst maintaining stiffening effects and maximising the stress transfer at the overmoulding interface. This is approached by moving the continuous fibre insert to the centreline of the panel to avoid warping, while reconfiguring the overmoulding material to maintain stiffness benefits and address fibre wash.

Initially, stress transfer at the end of the insert is investigated by using literature-derived material properties combined with Shear Lag theory to explore the parallels between a single fibre embedded in a matrix and a continuous fibre insert embedded in a short fibre filled matrix (Sections 2.1 and 2.2). While strength is not typically a primary driver for these components, damage caused by tensile loading (such as interface or interlaminar cracks) could lead to a knock down in bending performance. Furthermore, using an over-engineered insert would incur needless added cost.

Analytical and numerical methods are used to obtain an indication of the tensile behaviour for an insert when using a regular cross-section. This is expanded into a parametric finite element study using a range of material pairings to consider the effects of insert positioning within the part and the sensitivity of the tensile and bending behaviour to the relative dimensions of the insert and the overmoulding material.

Subsequently, a modified geometry with equal mass is proposed as a means of resolving manufacturing issues (warp, wash), while providing equivalent bending stiffness to the conventional Bias case (Section 2.3). The concept of an insert efficiency factor is introduced (Section 2.4) to aid material selection for both the insert and the overmoulding

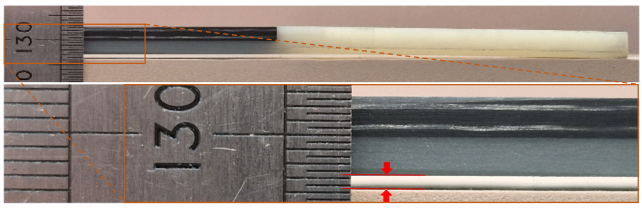

Fig. 1. Example of warping in a glass filled PA6 overmoulded part caused by the non-symmetric, 'Bias' placement of a quasi-isotropic carbon fibre reinforcing insert. The 86 mm long insert has caused approximately 2 mm of deflection (red arrow) in the centre of a 235 mm long specimen. (For interpretation of the references to colour in this figure legend, the reader is referred to the web version of this article.)

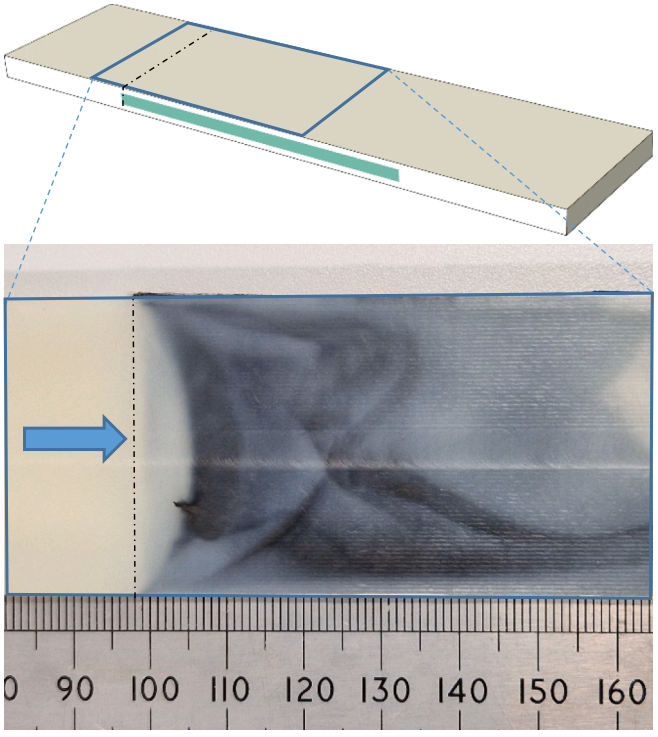

Fig. 2. Example surface wash in a glass filled PA6 overmoulded part with a centrally placed quasi-isotropic carbon fibre insert, with the injection flow direction indicated by an arrow. The deformation of the upper layers of the insert caused by flow of the overmoulding material across the insert surface is evident (referred to as 'wash').

materials. Theoretical data is compared to physical results in order to compare the models with physical components (Section 2.5).

For the purposes of this study, the models are idealised and limited to the elastic region. It is assumed that there is perfect bonding of the interface, that there is no deformation of the insert caused by manufacturing, and that the in-plane fibre orientation distribution in the short fibre overmoulding material is homogenised and random. This simplifies the assessment to enable the geometrical effects to be isolated at this stage, which is expected to demonstrate potentially significant deviation from real physical data. Subsequent studies will incorporate interface data, fibre orientation distribution and explore the region of plastic deformation.

2. Methodology

2.1. Material definitions for finite element modelling

In general, there were two material types in the composite components used in this numerical study: a unidirectional, continuous fibre-reinforced organosheet (the insert) and a short fibre-reinforced overmoulding compound.

For the majority of the simulation studies, the insert material was selected to be a unidirectional (UD) continuous fibre reinforced organosheet, using either carbon or glass fibres in a PA66 matrix. In the simulations, the insert materials were assumed to be transversely isotropic, and were modelled using an elastic material model. The fibre volume fractions of the insert material were selected to be 40 % and 60 % to investigate the influence of insert material properties on mechanical performance. The values of 40 % and 60 % were taken as practical upper and lower bounds for fibre content. The corresponding properties were calculated based on the approach used by Qui et al. [21,22] and are provided in Table 1. E_2 and E_3 were calculated according to Jacquet [23].

The overmoulding material was selected to be a PA66 matrix, containing short reinforcing fibres (0.15 mm) of either glass or carbon. In the simulation, the overmoulding material was considered to be isotropic and was also modelled as a purely elastic material. The fibre orientation distribution was assumed to be 2D random in-plane (a Krenchel orientation factor (η) of 0.375, where $\eta = \Sigma\, a_n \cos^4\Theta$ with Θ being the angle between the fibre direction and the loading direction and a_n the proportion of fibres at that angle) when calculating the modulus values, as the membrane stresses (in-plane stress) dominated the mechanical behaviour of the specimen due to the fountain flow behaviour of the injection moulding material. Fountain flow is a common phenomenon in injection moulding whereby the variation of flow and shear rate across the flow front results in a layered structure with very low occurrence of out-of-plane fibres [24,25]. The fibre mass fractions of the overmoulding material were selected to be 40 % and 60 % (mass fractions are more commonly used than volume fraction when referring to injection moulded materials). The corresponding properties were approximated according to the Rule of Mixtures, assuming ideal fibre distribution and perfect interfaces, and are listed in Table 2.

In addition to the parametric studies for these materials, additional simulations were performed to compare the results against physical specimens. Two material pairings were considered: a 45 % V_f carbon/PA6 continuous fibre insert coupled with a 35 wt% glass/PA6 overmoulding compound and a 45 % Vf carbon/PA6 continuous fibre insert coupled with a 30 wt% carbon/PA6 overmoulding compound. The properties for these materials are also provided in Tables 1 and 2.

Table 1
Mechanical properties for various insert materials, including 45CI used for validation. Designation indicates fibre volume fraction (40, 45, 60) and insert material type (CI – carbon insert, GI – glass insert). Values established using data from [32–37].

Material label	40CI	45CI	60CI	60GI
Material	Carbon/PA66	Carbon/PA6	Carbon/PA66	Glass/PA66
Volume fraction	40 %	45 %	60 %	60 %
Density (g/cm^3)	1.388	1.419	1.512	1.998
E_1 (GPa)	98.22	109.41	145.48	44.93
E_2, E_3 (GPa)	5.35	4.33	10.35	9.55
Nu_{12}, Nu_{13}	0.356	0.335	0.334	0.289
Nu_{23}	0.400	0.372	0.400	0.400
G_{12}, G_{13} (GPa)	3.12	2.52	4.44	5.49
G_{23} (GPa)	2.12	1.65	2.97	3.36
σ_b (MPa)	1455	1628	2147	1229

2.2. Critical insert length - parametric study

Cox's Shear Lag theory is commonly used to account for the aspect ratio of a discontinuous reinforcing fibre within a matrix material [26], providing expressions to calculate the axial fibre stress and the shear stress at the fibre/matrix interface. Unlike continuous fibre composites, the isostrain assumption used to calculate the effective composite stiffness (rule of mixtures) does not hold true for discontinuous fibre systems, since the fibres are indirectly loaded through shear mechanisms at the fibre/matrix interface. The mismatch in strain between the fibre and the matrix is a function of the position along the fibre and the radial distance from the fibre, which are both dependent on the ratio of the fibre modulus and the matrix modulus. There is a readily apparent comparison that can be made between the isolated, discontinuous fibre in Cox's model [27] and insert overmoulding, assuming a Symmetric insert configuration (Fig. 3a). The Cox model is a useful means of determining the relative stress distribution in and around the insert and can be used to form the basis of an efficiency factor (see section 2.4.1). This factor can be used to understand the required insert length to maximise the tensile stress carried by the insert fibres before failure occurs at the junction between the overmoulding material and the end of the insert.

To investigate tensile behaviour in insert overmoulding, both analytical and numerical methods were applied. For the numerical model, a uniaxial tensile test was applied by uniformly fixing one of the surfaces at the short edge, while a uniformly distributed tensile load was exerted onto the opposite surface. The data for this study was extracted from the central xz plane in Fig. 3a. The analytical approach applied the Cox model by directly substituting the monolithic fibre with the continuous fibre composite insert. Properties for the insert were taken from Table 1 and an idealised hexagonal packing arrangement was assumed to calculate the tensile stress.

The size of the insert was varied in 10 % increments of both the total length and the total thickness of the overall specimen, between values of

Table 2
Mechanical properties for overmoulding material, including materials used for validation. Designation indicates fibre mass fraction (35, 40, 60) and overmould material type (CO – carbon overmould, GO – glass overmould). Values established using data from [32–37].

Material label	40CO	40GO	60GO	35GO	30CO
Material	Carbon/PA66	Glass/PA66	Glass/PA66	Glass/PA6	Carbon/PA6
Mass fraction	40 %	40 %	60 %	35 %	30 %
Volume fraction	30 %	23 %	40 %	19 %	22 %
Density (g/cm^3)	1.327	1.466	1.711	1.416	1.275
E (GPa)	15.44	7.07	9.97	5.25	9.20
Nu	0.367	0.358	0.326	0.342	0.354
Yield stress (MPa)	221*	201*	232*	185	214

*Yield values based on averages for similar commercial materials in Matweb database tested to ASTM D638.

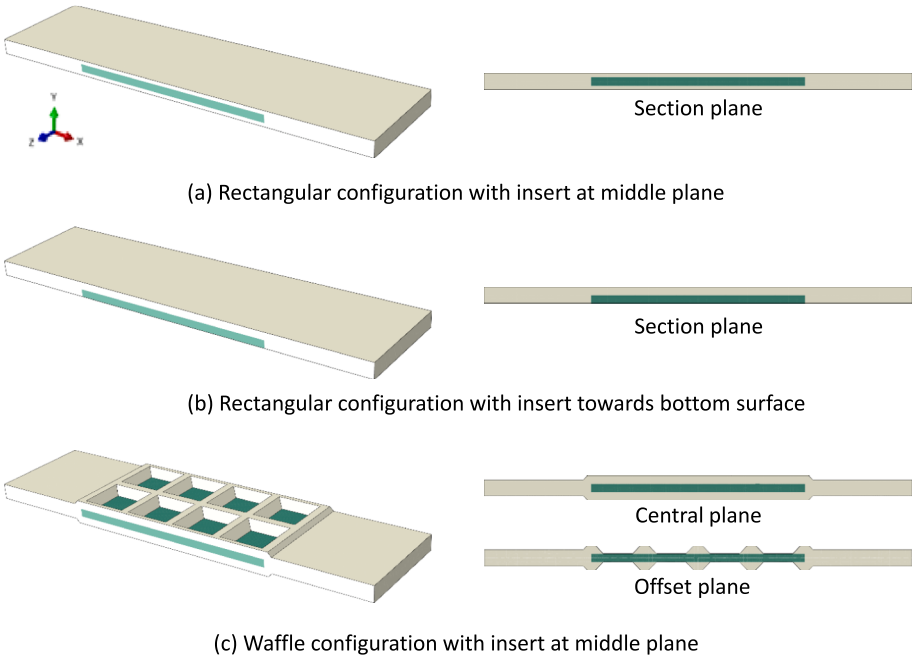

Fig. 3. Three different geometries investigated in tension and bending: (a) symmetric positioning equivalent to the Shear Lag configuration; (b) Bias positioning representative of the standard insert moulding configuration; (c) the Waffle configuration.

Table 3
Material pairings used in Shear Lag assessment.

Material pair code	Insert material	Overmoulding material
40CI40CO	40 % V_f carbon	40 % carbon by mass
40CI40GO	40 % V_f carbon	40 % glass by mass
40CI60GO	40 % V_f carbon	60 % glass by mass
60CI40CO	60 % V_f carbon	40 % carbon by mass
60CI40GO	60 % V_f carbon	40 % glass by mass
60CI60GO	60 % V_f carbon	60 % glass by mass
60GI40CO	60 % V_f glass	40 % carbon by mass
60GI40GO	60 % V_f glass	40 % glass by mass
60GI60GO	60 % V_f glass	60 % glass by mass

20 % and 80 %. Nine different material pairings were considered, as shown in Table 3. The pairings were selected to provide parts with a range of overall stiffness values. This provided a total of 441 configurations.

2.3. *Modified overmoulding design – Waffle geometry*

A modified geometry is proposed in order to address both manufacturing issues and to manage the transition of stress at the ends of the insert. This geometry is referred to as the 'Waffle' configuration. The overmoulding material covering the large planar surfaces of the insert in Fig. 3a and 3b carries significantly less stress than the insert, since the insert material is generally much stiffer than the overmoulding material. The Waffle geometry (Fig. 3c) redistributes this volume of overmoulding material to provide a more gradual stress transition at the ends of the insert. It also increases the overall second moment of area for the hybrid panel, improving the bending resistance to compensate for the central positioning of the insert.

The central location of the insert provides a more balanced structure for moulding, greatly reducing the likelihood of warpage as the part cools, in comparison to the Bias insert. The large draft angle also provides ease of demoulding and the Waffle structure increases the direct clamping area of the tool face in the form of 'pinch' points, providing resistance to 'wash' on filling. This large contact area also facilitates heat conduction to the insert from both tool faces, potentially improving interfacial bonding in the surrounding regions.

The dimensions of this Waffle structure can be varied through a number of parameters in order to improve the performance of the transition region, including rib height and width, rib angle and position in relation to the end of the insert, but this extensive optimisation is beyond the scope of the current study. A simple initial case was used with a fixed 45° angle to the Waffle (see Fig. 4).

2.3.1. *Waffle equal mass calculation*

Utilisation of the Waffle geometry should not incur additional mass, and so the design of the geometry was adjusted to ensure that an equivalent amount of material was used in the Waffle as in the continuous cross section. This was achieved by controlling the height, the angle and the spacing between the ribs (see Fig. 4).

A unit cell of the Waffle structure was generated to establish a relationship between the Waffle height and the distance between the ribs, assuming a 45° wall angle (Equation 1).

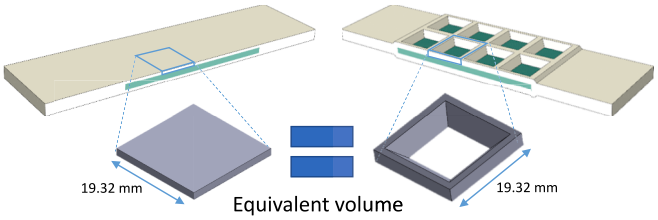

Fig. 4. The continuous cross section (left) has an equivalent volume to the Waffle unit cell (right).

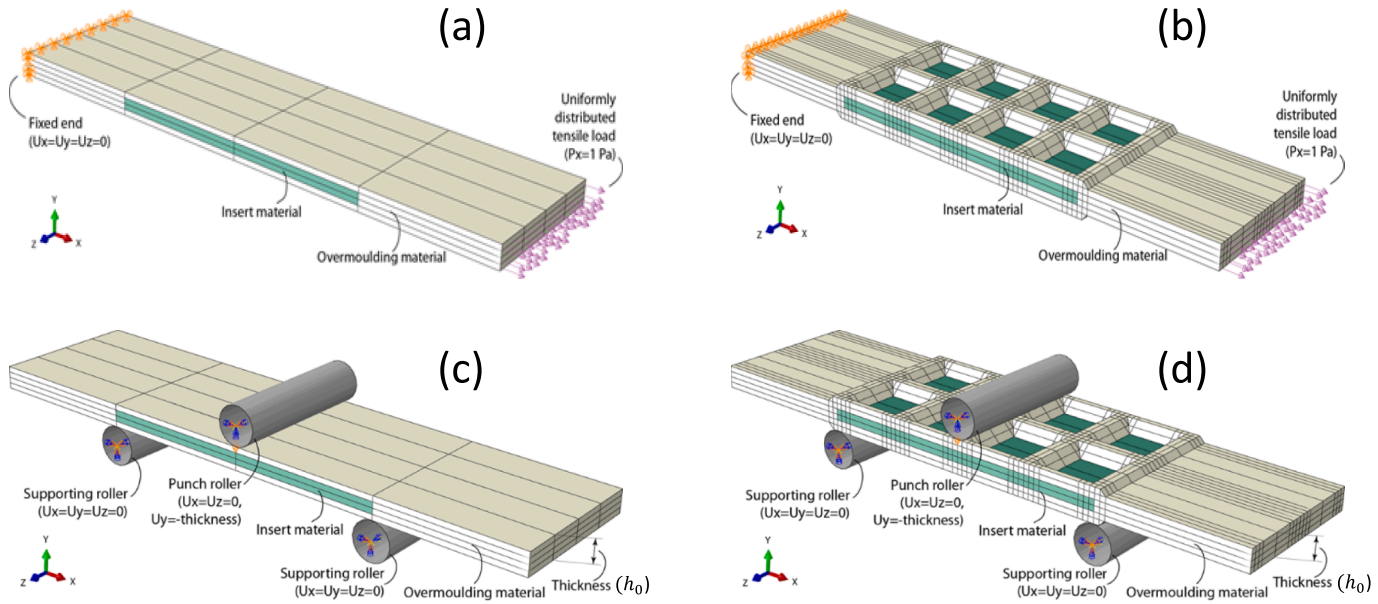

Fig. 5. Schematics of numerical models (a) longitudinal extension of Symmetric configuration (similar for Bias configuration), (b) longitudinal extension of Waffle configuration, (c) out-of-plane bending of Symmetric configuration (similar for Bias configuration), (d) out-of-plane bending of Waffle configuration.

$$\text{Distance between ribs} = x + \sqrt{\frac{22x^2}{3}}, \text{ where } x \text{ is the height of the Waffle rib.} \tag{1}$$

2.3.2. Waffle structure parametric study

As shown in Fig. 5, a numerical model was created to simulate longitudinal in-plane tension and out-of-plane bending tests for the Bias and Waffle geometries. The in-plane dimensions of the specimen section were fixed to be 38.64 mm × 5.76 mm (for the non-Waffle region) and × 8.64 mm (for the Waffle region). The length of the sample was 172 mm, with the Waffle region being 85.92 mm long (including 4 × 19.32 mm Waffle sections, plus the additional end ribs of 2 × 4.32 mm). A reduced set of configurations was considered in this study, with the insert fixed at 50 % of the total thickness of the component. Abaqus/Standard 2018 was used for the finite element analysis, using 10-noded tetrahedral continuum elements (C3D10) with an average edge length of 0.5 mm.

For the tensile test, one of the surfaces along the short edge was fixed (Ux = Uy = Uz = 0) and a uniformly distributed tensile unit load was exerted on the opposite surface.

For the bending analysis, the specimen lay on two supporting rollers with a span of 80 mm in between. The 3rd moving roller was placed at the middle of the span between the two supporting rollers, but with contact established from the other side. A vertical displacement equal to the thickness of the specimen was applied to the punch roller during the simulation, causing the specimen to bend.

2.4. Evaluation methods

2.4.1. Tensile simulations

- *Material efficiency*

Both the insert and overmoulding materials were assumed to be elastic in the FE simulations and so the stress could be linearly scaled for increasing values of applied strain. The overmoulding material was expected to yield prior to failure of the insert material, as the yield stress of the overmoulding material is typically much lower than the insert σ_b (see Tables 1 and 2). At the point at which this yielding occurs, the stress in the insert material could be recorded and used to determine the 'insert efficiency factor' or ϵ_{eff}, which is defined as:

$$\epsilon_{eff} = \frac{\sigma^{IN}_{max}}{\sigma^{IN}_{b}} \tag{2}$$

where, σ^{IN}_{max} denotes the maximum stress in the insert material when the component starts to yield and σ^{IN}_{b} denotes the expected ultimate tensile stress (UTS) of the insert material. The value of σ^{IN}_{max} is limited by the occurrence of yielding in the overmoulding material as it reaches its yield stress σ^{OM}_{Y}. Since the stress can be linearly scaled in an elastic model, a scaling factor $f_{scaling}$ can be calculated as:

$$f_{scaling} = \frac{\sigma^{OM}_{Y}}{\sigma^{OM}_{FE,max}} \tag{3}$$

where, σ^{OM}_{Y} denotes the yield stress of the overmoulding material, and $\sigma^{OM}_{FE,max}$ denotes the maximum stress of the overmoulding material from the FE simulation. The maximum stress of the insert material σ^{IN}_{max} can be calculated as:

$$\sigma^{IN}_{max} = f_{scaling} \bullet \sigma^{IN}_{FE,max} \tag{4}$$

where $\sigma^{IN}_{FE,max}$ denotes the maximum stress of the insert material from the FE simulation.

Therefore, the material efficiency ϵ_{eff} can be determined by

$$\epsilon_{eff} = f_{scaling} \bullet \frac{\sigma^{IN}_{FE,max}}{\sigma^{IN}_{b}} = \frac{\sigma^{OM}_{Y} \bullet \sigma^{IN}_{FE,max}}{\sigma^{IN}_{b} \bullet \sigma^{OM}_{FE,max}} \tag{5}$$

- *Maximum tensile load*

The maximum tensile load $C_{load}^{tensile}$ can be described using the maximum external force when the entire component starts to yield. Therefore, $C_{load}^{tensile}$ is obtained as

$$C_{load}^{tensile} = f_{scaling} \bullet L_{FE} = \frac{\sigma_Y^{OM} \bullet L_{FE}}{\sigma_{FE,max}^{OM}} \tag{6}$$

where L_{FE} denotes the external load applied to the component in the FE simulation.

The ratio between ϵ_{eff} and $C_{load}^{tensile}$ is

$$\frac{\epsilon_{eff}}{C_{load}^{tensile}} = \frac{\sigma_{FE,max}^{IN}}{L_{FE} \bullet \sigma_b^{IN}} \tag{7}$$

where L_{FE} is determined by the loading condition; $\sigma_{FE,max}^{IN}$ is derived from the elastic deformation behaviour that depends on the distribution of elastic modulus across the entire component; σ_b^{IN} is determined by the material strength. Herein, the use of the strength of the insert material was based on the assumption that material yielding commences from the overmoulding material. Therefore, the mechanical performance of the component is dominated by the geometry of the component and the ratio of the elastic material properties between the insert and the overmoulding materials.

2.4.2. Bending simulations

A maximum vertical displacement ($d_{FE,max}^{punch}$) equal to the thickness of the specimen (h_0) was applied to the punch roller in the FE simulation. The maximum reaction force from the punch roller (i.e. $R_{FE,max}^{punch}$) can be obtained from the simulation. Since the materials in the FE model were assumed to be elastic, this reaction force (R^{punch}) corresponds to an arbitrary displacement (d^{punch}) at the mid-span and can be scaled linearly as follows:

$$R^{punch} = R_{FE,max}^{punch} \bullet \frac{d^{punch}}{d_{FE,max}^{punch}} \tag{8}$$

where, $d_{FE,max}^{punch} = h_0$ herein and d^{punch} should be small to ensure the material deforms within the elastic range. Consequently, the larger the reaction force R_{FE}^{punch}, the higher the maximum load-carrying capacity in bending.

Thus, the maximum bending load $C_{load}^{bending}$ is

$$C_{load}^{bending} = R_{max}^{punch} = R_{FE,max}^{punch} \bullet \frac{d_{max}^{punch}}{h_0} \tag{9}$$

where, R_{max}^{punch} is the reaction force from the punch roller, d_{max}^{punch} is the maximum vertical displacement applied to the punch roller.

In addition, the bending stiffness ($k^{bending}$) is another performance indicator, which can be obtained by measuring the slope of the load versus deflection curve, i.e. the punch roller reaction force versus the vertical displacement.

2.5. Physical specimens

2.5.1. Manufacturing

Physical specimens were produced by Surface Generation Ltd. (SG) following the process shown in Fig. 6. The samples were produced at a nominal length of 235 mm (tool dimension) to allow additional material for gripping in the tensile tests. The short fibre granules (30 wt% carbon fibre filled Opti-Polymer 4121 WPZ- PA6 CF30 ST schwarz 16–1377 V and 35 wt% glass fibre filled BASF UltramidB3EG7) were dried according to the datasheet provided by the manufacturers using a Summit Systems DryPlus 025. The 2.88 mm thick laminate inserts were manufactured from SGL PA6/CF tape utilising Sigrafil C T50 fibre at 45 % volume fraction.

Flat panels were produced using matched die tooling incorporating SG's PtFS technology, mounted to the platens of a hydraulic platen press providing up to 100 t of clamping force. Laminate preforms were heated to 265 °C, held at this temperature for 4 min and then cooled to below 80 °C for demoulding. A consolidation pressure of 40 bar was applied halfway through the 4-minute dwell at 265 °C, which was held until demoulding. The laminates were cut into the required insert shapes using an abrasive water jet cutter. These inserts were dried prior to overmoulding under the same conditions as the granules.

The interface surface was cleaned with isopropanol and heated in an oven at 60 °C for a minimum of 10 min prior to overmoulding. Inserts were manually positioned in the overmoulding tool. Location of the insert was achieved using a rebated geometry. Where necessary, retention of the insert was achieved using fixated tooling tabs.

The injection moulding machine was an Engel Victory 120. This provided a maximum shot volume of 250 cm^3 and a maximum injection (melt) pressure of 130 MPa. The maximum clamp force available was 120 t. The barrel temperature ranged from 270 °C to 285 °C and the hot runner temperature was 300 °C. The tool temperature was held at 160 °C and the injection barrel speed was 10 mm/s. Switch over from filling to packing was set to 10 mm from full stroke. A typical holding cycle was 42 MPa for 10 s.

Samples were stored in an oven at 60 °C after demoulding and allowed to cool down to ambient temperature overnight.

2.5.2. Mechanical testing

Physical specimens were assessed in tension and 3 point bending on

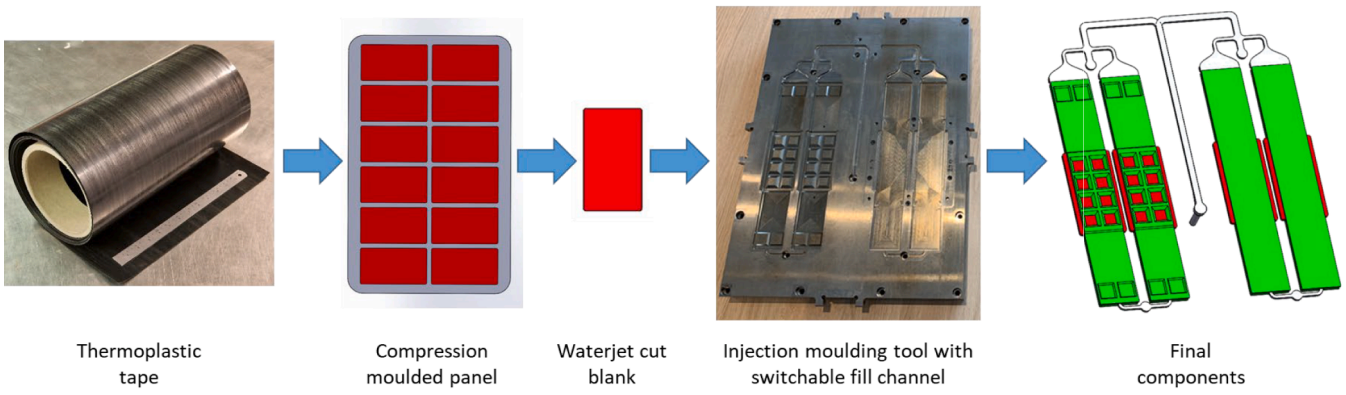

Fig. 6. Schematic of the process followed for the production of the physical test specimens with Bias and Waffle insert positions, using injection overmoulding.

an Instron 5581 testing frame, using a 50 kN load cell and a crosshead displacement rate of 1 mm/min. Textured wedge grips were used for tensile testing, with approximately 30 mm of material held in each grip such that there was 172 mm of sample between the grips to match the model loading case. A Limess Vic3D digital image correlation (DIC) strain measurement was used in combination with Pentax C7528-M cameras providing 1638 × 1066 pixel images. The cameras were positioned approximately 1 m from the samples with an angle of 30° between the cameras. A pre-optimised speckle pattern was applied to a water transfer film [28] and the stereo images taken during the test were analysed using the Vic-Software. The 3-point bend test used Ø10 mm rollers and a test span of 80 mm (from end rib to end rib), with strain measured using a calibrated iMETRUM digital video gauge (accuracy taken as ± 0.5 %). By placing the rollers at the rib positions, the effect of the Waffle cross-section could be assessed against the Bias without being influenced by the stress concentrations at the insert ends.

2.5.3. Microscopy

Microscopy samples were embedded in Synolite resin, with a maximum exotherm of 50 °C. Sample blocks were ground flat and parallel before sequential polishing from 400 to 4000 grit and final lapping using a 1 μm alumina suspension. Tiled images were collected using a Leica microscope and Image-pro software.

3. Results and discussion

3.1. Parametric study of tensile behaviour in Symmetric configuration: Shear lag analysis versus FE analysis

For each case, the direct stress (S11) along the longitudinal direction was extracted from the finite element model along the centreline of the Symmetric insert configuration and then compared to the results from the analytical Shear Lag model (see Fig. 7). There is a clear correlation between the two approaches, giving confidence that the simple analytical method could provide a reasonable approximation of the axial tensile stresses within the insert without the need for more sophisticated modelling. However, there are obvious limitations. The analytical model assumes that the tensile stress at the ends of the insert is zero, which contradicts experimental studies focussing on single fibres. Previous studies on single fibres suggest that strains at the end of the reinforcement are negligible as Ef/Em tends to 100 (as is the case for a single carbon fibre embedded in epoxy) [29]. However, these strains become more significant as the ratio of E_f/E_m decreases, as shown by Galiotis et al. [30], who reported strains of up to 0.5 % at the fibre ends when E_f/E_m was 16.

These stresses and strains are therefore too significant to ignore, particularly for inserts with low aspect ratios (length / thickness). Furthermore, the Shear Lag theory imposes no constraints on the matrix thickness, whereas the insert thickness in this case is of a finite depth. Due to these factors, the critical length values started to diverge when the insert reached around 30 % of the thickness of the component (results not presented here). Consequently, an analytical prediction only appears to provide a reasonable result for thin inserts (up to ~ 20 % of the thickness, as shown in Fig. 7). The analytical model also assumes the specimen is symmetrical about the mid-plane and for these reasons, subsequent studies have used the finite element approach.

From the FE data in Fig. 7a, it can be seen that the stresses observed at the ends of the insert were on the order of 450 – 500 MPa, which are expected to be well above the yield values of the overmoulding material (on the order of 200 – 250 MPa according to Table 2). This indicates that, as expected, the system would fail in the region of pure overmould. These values can be scaled to the value of the yield stress, to obtain a more realistic maximum stress in the insert that can be used to assess material efficiency.

3.2. Material efficiency under uniaxial extension

The tensile behaviour confirmed that it would be very unlikely that the insert would fail in tension before the surrounding overmoulding material yielded. The concept of an “insert efficiency factor” (see Section 2.4) is proposed, which can be used to assess the peak load carried by the insert before failure occurs within the bulk overmoulding material. The ‘efficiency’ of the insert can be used during material selection to evaluate cost versus performance.

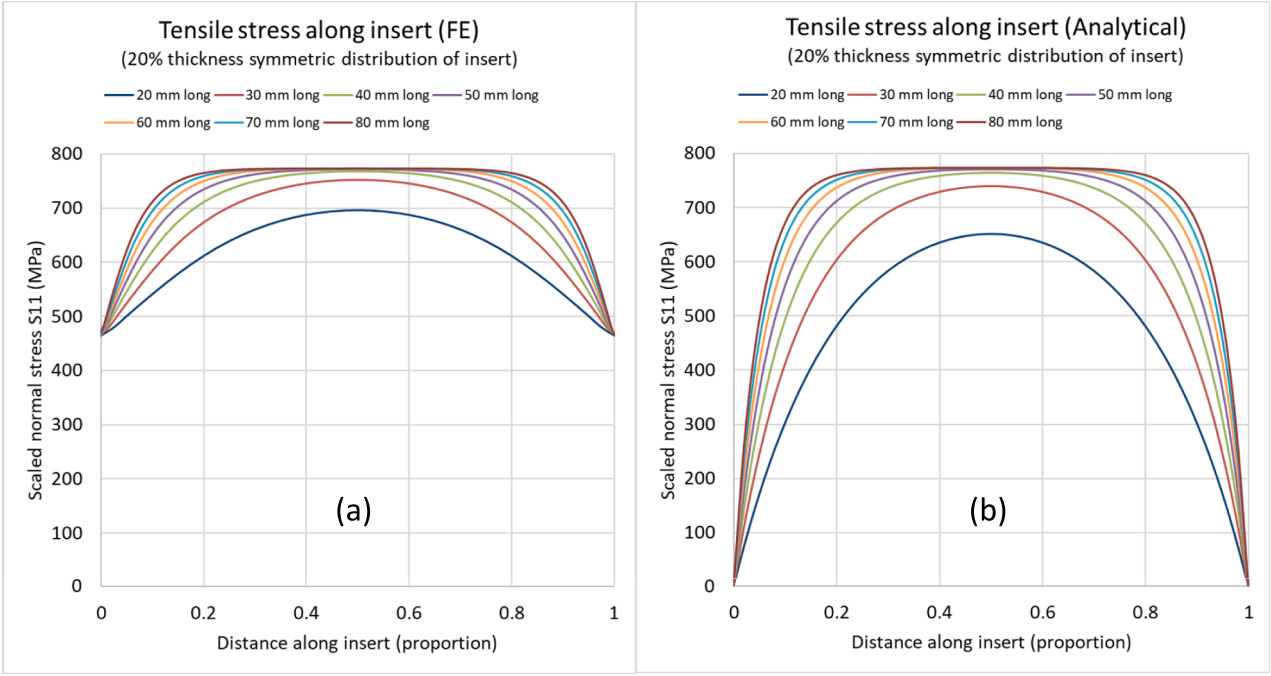

Fig. 7. Example of results for S11 tensile stress along the centreline of the insert, for an insert that is 20 % of the total thickness of the component. (a) Results from finite element model. (b) Results from analytical model.

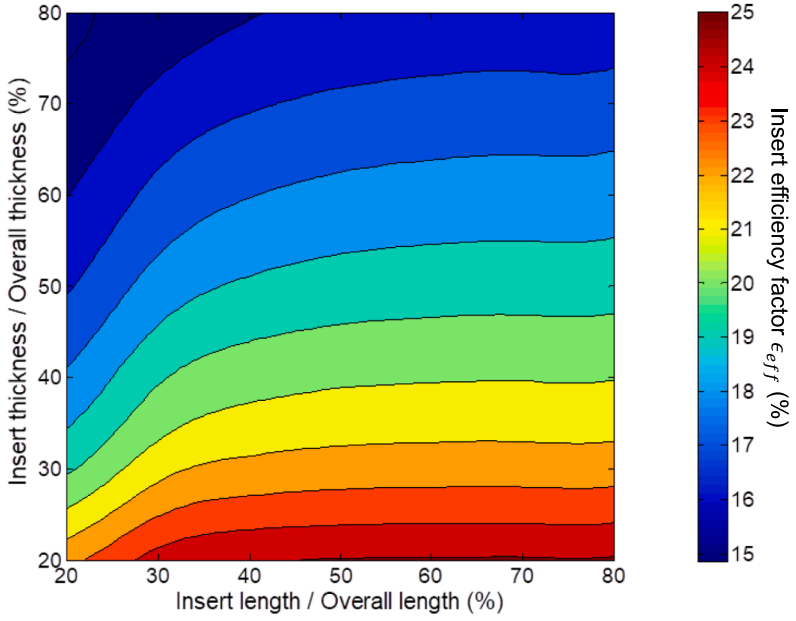

Fig. 8. Surface plot of insert efficiency factor ϵ_{eff} for the material pairing 40CI 40CO as a function of relative thickness and relative length of the insert with respect to the part dimensions. Symmetric positioning of insert (see Fig. 3a).

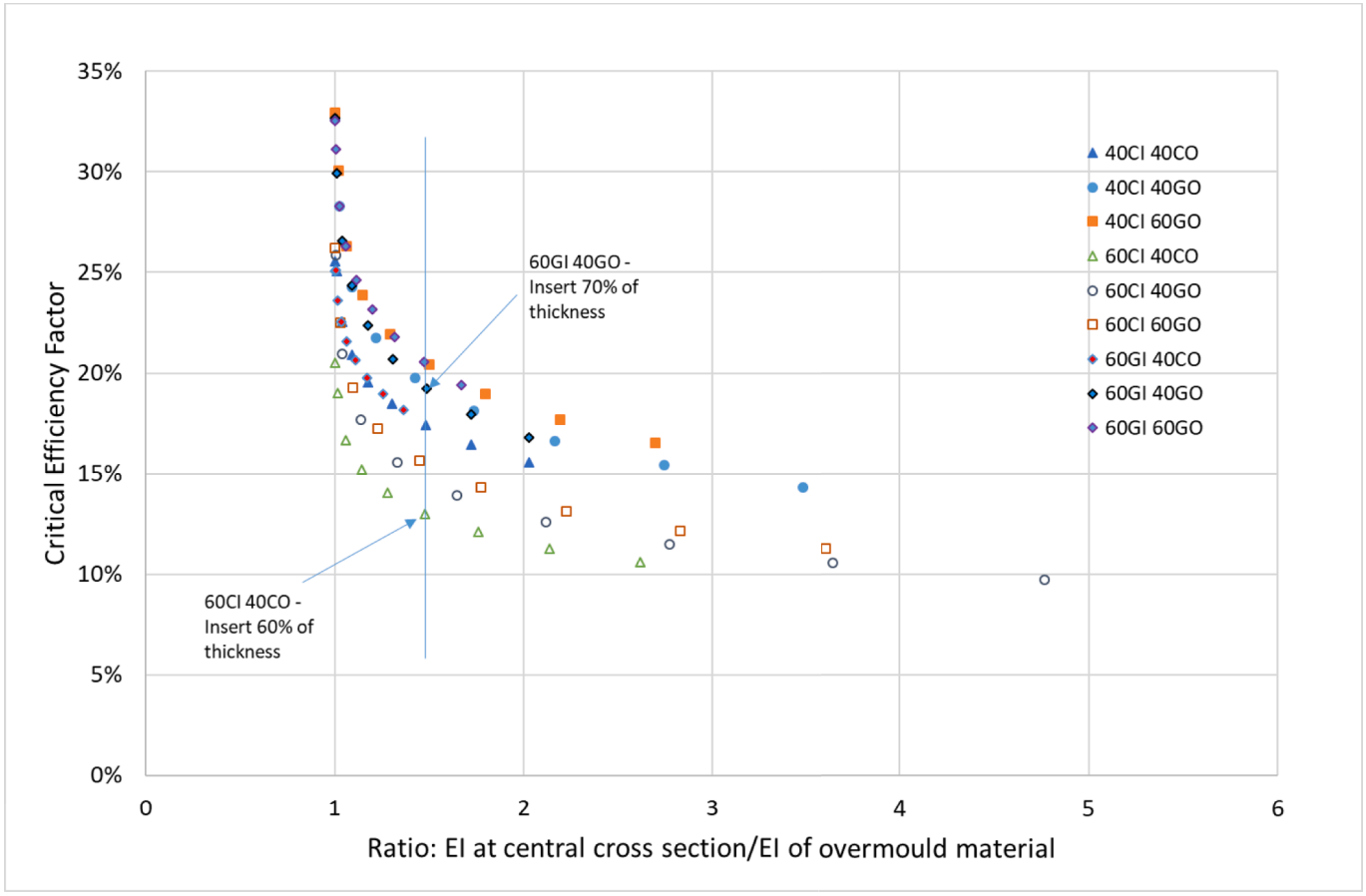

Fig. 9. Critical insert efficiency factor as a function of the ratio of the EI of the central cross section to the EI of the overmoulding material alone. The ratio on the x axis provides an indication of increasing insert thickness and stiffness. Insert configurations are 10–90 % of the total specimen thickness. Two materials are highlighted with equivalent stiffness profiles, with one making more efficient use of a slightly thicker glass insert (20 %) instead of a slightly thinner carbon insert (13 %).

It was observed in the FE analyses that stress concentrations occurred in the overmoulding material at the junction with the insert. By scaling this peak stress to the yield value of the overmoulding material, the maximum direct stress values along the centreline axis of the insert (S11) could be scaled by a similar factor and compared with the properties of the insert. In doing so it is possible to determine what proportion of the maximum insert properties would be utilised before the part failed, which is noted as an insert efficiency factor (ϵ_{eff}) (Equation (2). For each material pairing, a surface plot can be generated relating ϵ_{eff} to the geometry in terms of thickness and length. An example is provided in Fig. 8 for the 40CI 40CO material pair. It should be noted that this calculation is performed based on a model that assumes perfect interfacial bonding, and so is valid only when failure is as a result of the polymer yielding and not a cohesive failure due to debonding.

It can be seen from Fig. 8 that the ϵ_{eff} values for a given pairing reach a plateau value with length, suggesting a critical ϵ_{eff} can be determined using an approach analogous to that of the Shear Lag critical length. These critical ϵ_{eff} were determined for each insert thickness and for each material pairing and are plotted in Fig. 9. The critical ϵ_{eff} values are plotted against a normalised value of rigidity (EI), where the calculated EI of the central cross-section of the part is divided by the EI for a sample made purely from overmoulding material (i.e. as if there was no insert).

The efficiency dramatically decreases as the stiffness ratio increases. This indicates that the most efficient use of a Symmetric insert configuration loaded in tension would be as a long, thin insert relative to the dimensions of the overmoulded section. The results indicate that different material combinations and geometries with similar stiffness are achieved that have different efficiency factors, providing engineers an opportunity to find an optimum cost/performance balance. For example, the same stiffness is achieved when using a 70 % insert thickness 60GI 40GO pairing or a 60 % insert thickness 60CI 40CO pairing, but less efficient use is made of the carbon insert in comparison with the glass (The carbon insert is only loaded to 13 % of its maximum capacity, while the glass is loaded to 20 %). It is worth pointing out that there would also be a difference in the mass for these two systems, as the glass fibre-based combination would be approximately 28 % heavier than the carbon fibre system.

It is apparent that using a discrete insert in a continuous section component does not provide satisfactory utilisation of the tensile properties of the expensive insert. Even in the best case, only 33 % of the peak tensile performance of the insert was used. An alternative component design should therefore be considered to ensure a more efficient use of the insert and to take advantage of the lower cost materials. This could include direct loading of the insert in a more conventional overmoulding configuration, or geometrical alterations such as the Waffle shape proposed in this paper, and/or the shape of the end of the insert itself. Such geometrical changes could potentially reduce the stress concentration at the material junction and enable greater stress transfer to improve the efficiency of the insert.

3.3. Bending case

While smoothing stress transitions to improve tensile behaviour and mitigation of warping effects are beneficial, in practice insert moulding is primarily driven by improvements in bending stiffness and so the Waffle structure must perform in this area. A key attribute of the Waffle configuration is that the insert has been moved from the face of the component to the centre, reducing its likelihood of warpage, but moving the higher stiffness element to coincide with the neutral axis. The intent is that the Waffle structure increases the overall second moment of area for the overmoulding material to compensate, but it is necessary to quantify the effect of these competing characteristics. Simulation of the bending case as per the approach shown in Fig. 5c and 5d was undertaken for each of the 9 material pairings in order to make this assessment. An example of the simulation data is provided in Fig. 10, where it is apparent that the majority of the stress is carried by the insert, as expected.

The reaction forces as a function of deflection were determined for

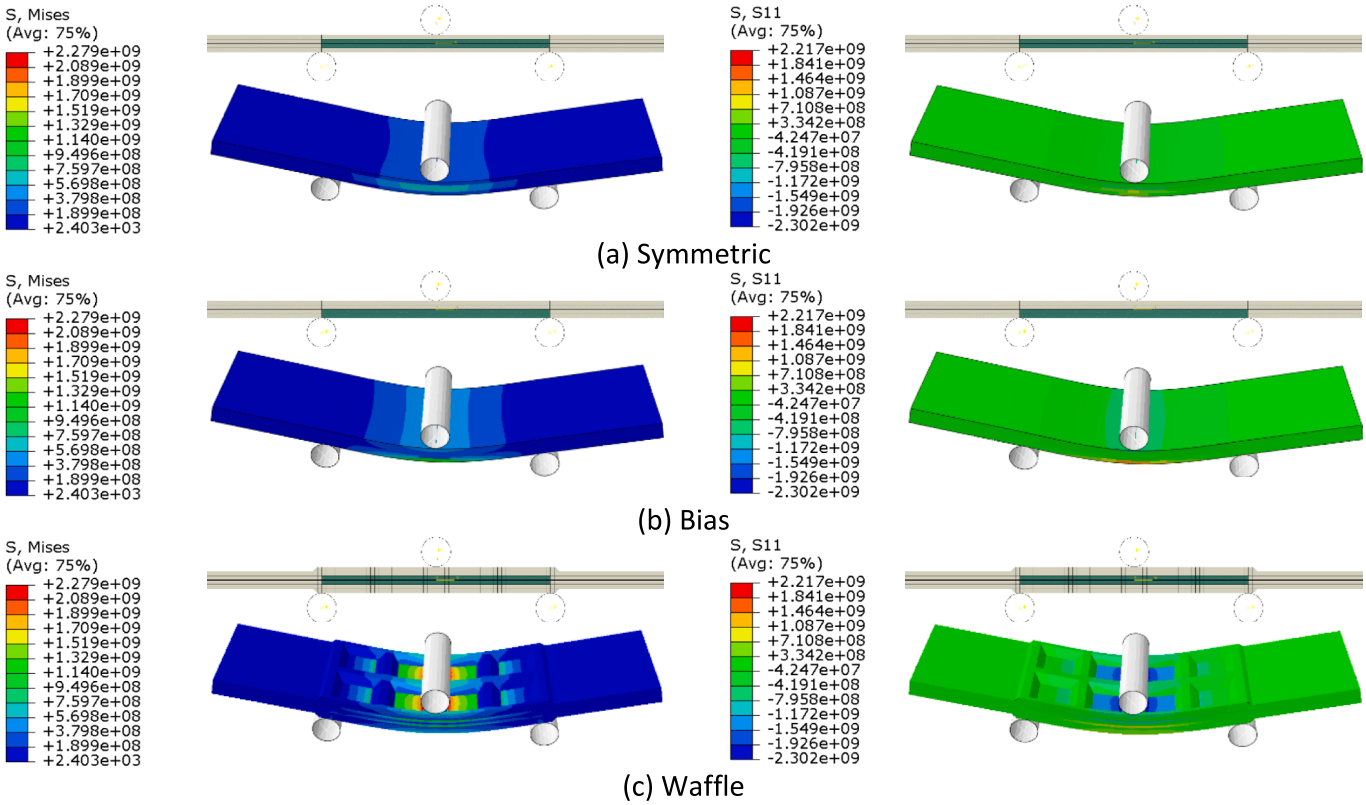

Fig. 10. Stress distribution in (a) Symmetric, (b) Bias and (c) Waffle cases under bending load. Example provided is for the 40CI40CO material pairing.

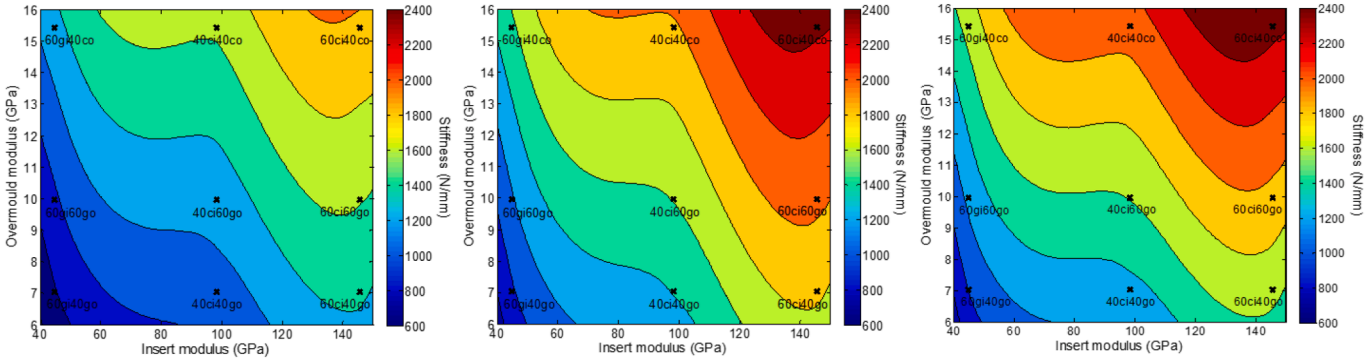

Fig. 11. Surface plots of stiffness as a function of overmould and insert modulus for the three configurations: Left to right – Symmetric, Waffle, Bias.

each of the 9 material pairings. The gradients of these force/deflection plots were used as an indication of the panel stiffness values, which were plotted as a function of the insert modulus and the overmoulding material modulus in Fig. 11. The stiffness of the Waffle configurations is similar to that of the Bias configuration in each case, in some cases exceeding it. This gives confidence that the Waffle configuration should have minimal impact on the bending stiffness of the part, whilst providing improved manufacturing characteristics. Both the Bias and Waffle configurations outperform the Symmetric case by 15–30 %.

3.4. Comparison with physical specimens

Physical specimens were produced to test the validity of the simulations and to explore the component behaviour beyond the elastic region. Two additional material pairings were simulated to compare to available physical materials – 45CI35GO and 45CI30CO (See Tables 1 and 2 for the properties used in the simulations). After manufacturing, the specimens were assessed for degree of warp along the length of the part. While the Bias case saw deformation on the order of 2 mm over the part length (see example Fig. 1), the symmetrical Waffle geometry reduced this warping effect to < 0.3 mm.

3.4.1. Tensile tests

Tensile data is provided in Fig. 12, showing the average yield and average maximum load for the Waffle and Bias specimens. This is presented alongside the neat overmoulding material as well as results from the model. The onset of failure was considered to have occurred when an element of the overmoulding material had reached the anticipated yield value (determined as an average of similar commercial material properties from the literature, shown in Table 2).

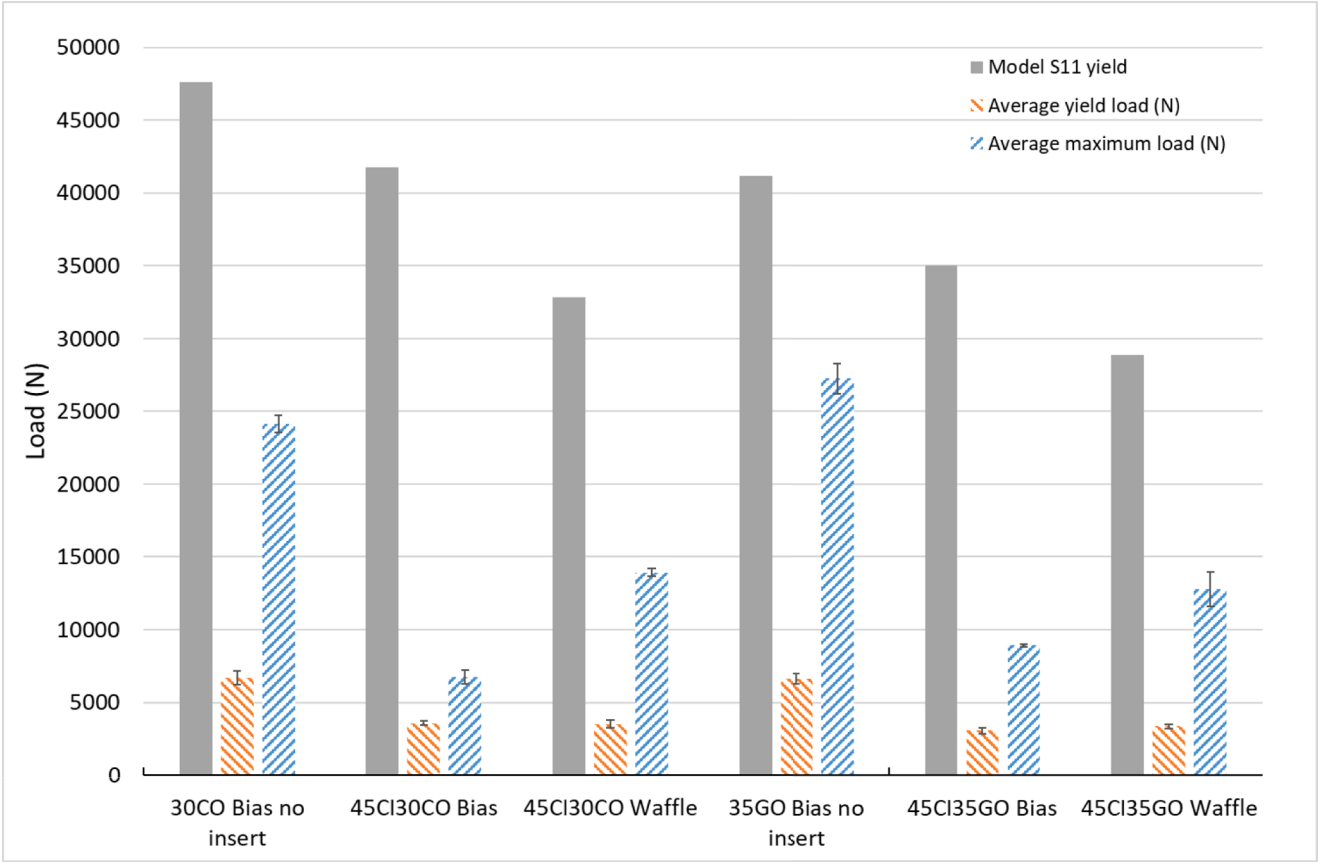

Fig. 12. Average yield and maximum load values for overmoulded specimens subjected to tensile testing, alongside predicted maximum load carrying capacity from the finite element model.

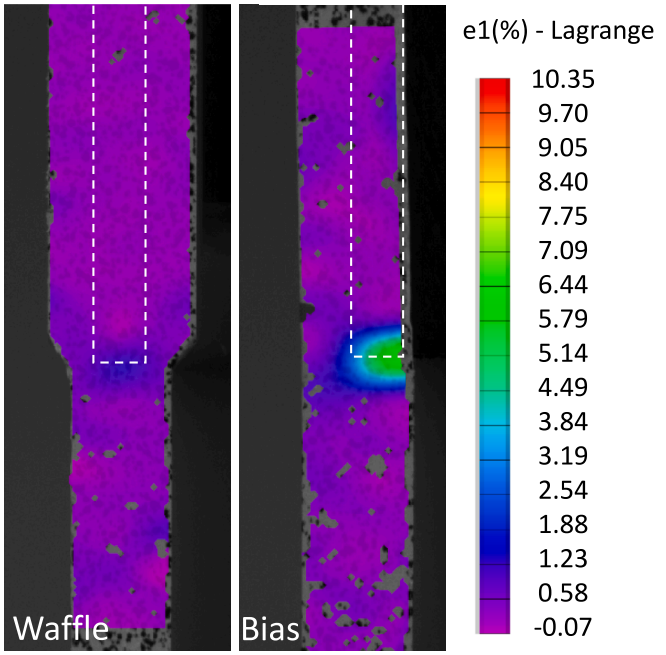

Fig. 13. Local strains recorded on the edge face of the specimen, determined via digital image correlation (DIC) for Waffle (left) and Bias (right) samples subjected to approximately 0.75 % global tensile strain. Approximate location of inserts shown by dotted lines.

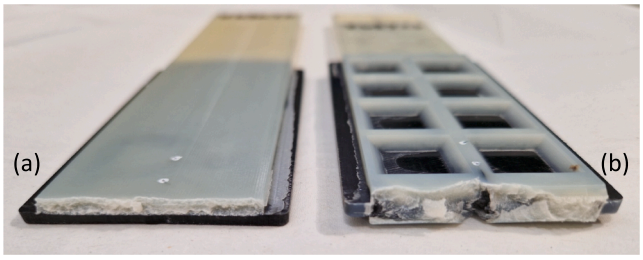

Fig. 14. Tensile failure behaviour examples for 45CI35GO material in (a) Bias and (b) Waffle configurations.

As expected, the tensile properties are reduced by the presence of an insert, due to the stress concentrations and matrix only bonding in the transition regions. The Bias and Waffle configurations exhibit similar yield values, while the Waffle has a significantly higher maximum load. According to Fig. 13, the Bias samples experience a strain concentration at the end of the insert that is 4 – 5 times higher than for the Waffle specimens, resulting in premature failure.

The failure area for the Waffle configuration is also larger than for the Bias specimens. As can be seen in Fig. 14a, the fracture site for the Bias specimens is relatively planar in line with the end of the insert. The fracture site for the Waffle specimens (Fig. 14b) is coarser across a broader area, exhibiting failure in the overmoulding material away from the end of the insert.

The simulation results from Fig. 12 appear to overestimate grossly the anticipated load at the yield point for the overmoulding material for the tensile case. This is in part due to an overestimation of the yield values for the overmoulding materials from the literature. Data produced from tensile dogbones was used, which tend to have preferential fibre alignment along the length of the specimen, increasing the Krenchel orientation efficiency factor beyond 0.375. The model also overlooks failure at the interface between the overmoulding material and the insert, which appears to be a dominant failure mode from the images in Fig. 14. The interface has much lower tensile properties than the fibre-filled overmoulding material, closer to an unfilled material and on the order of 1/3 the tensile yield strength.

The difference between the model and the physical specimens highlights the level of importance of the interface in the tensile case for both the Bias and Waffle configurations. The position of failure at the ends of the insert suggests that failure of the interface may be the initiator for part failure. If the interface is absent, the load is focused through a notch onto a cross-section that is half the area of the part (since the interface in these samples is 50 % of the cross-section). This effect might be mitigated by the use of tapered ends to the inserts, however this is not really feasible for small discrete inserts during layup and would perhaps need to be post-machined. Furthermore, general aerospace guidelines governing ply drops suggest that the length of the ply drop should be at least 8 times the ply thickness [31]. The specimens used in this study would therefore need an edge taper that would be approximately 25 % of the total length of the specimen at each end, which would also be impractical.

3.4.2. *Bending tests*

The bending stiffness data is provided in Fig. 15, alongside the predicted properties from the FE models. The prediction fits well to the Bias case, falling within one standard deviation of the experimental data, while the experimental Waffle specimens underperform in relation to the predicted values. Since the agreement for the simpler Bias case is generally good, there appears to be a factor of the Waffle configuration that has not been captured by the model. As noted in the introduction, the model assumes perfect interfacial bonding and uses a homogenised random in-plane fibre orientation distribution for the short fibres in the

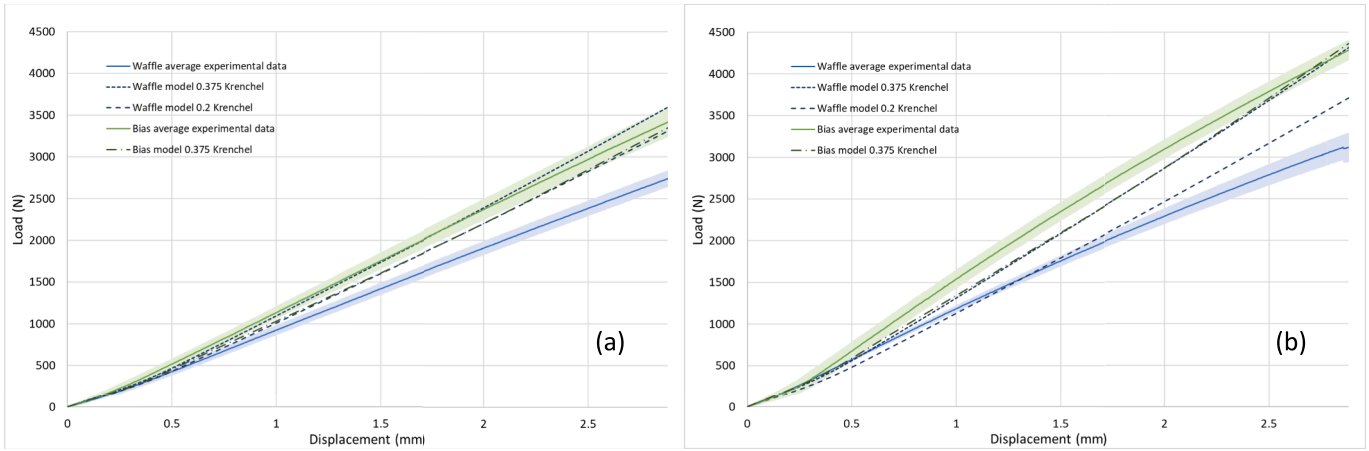

Fig. 15. Load/Deflection curves showing bending behaviour for (a) the 45CI35GO and (b) 45CI30CO physical specimens in comparison to the model cases.

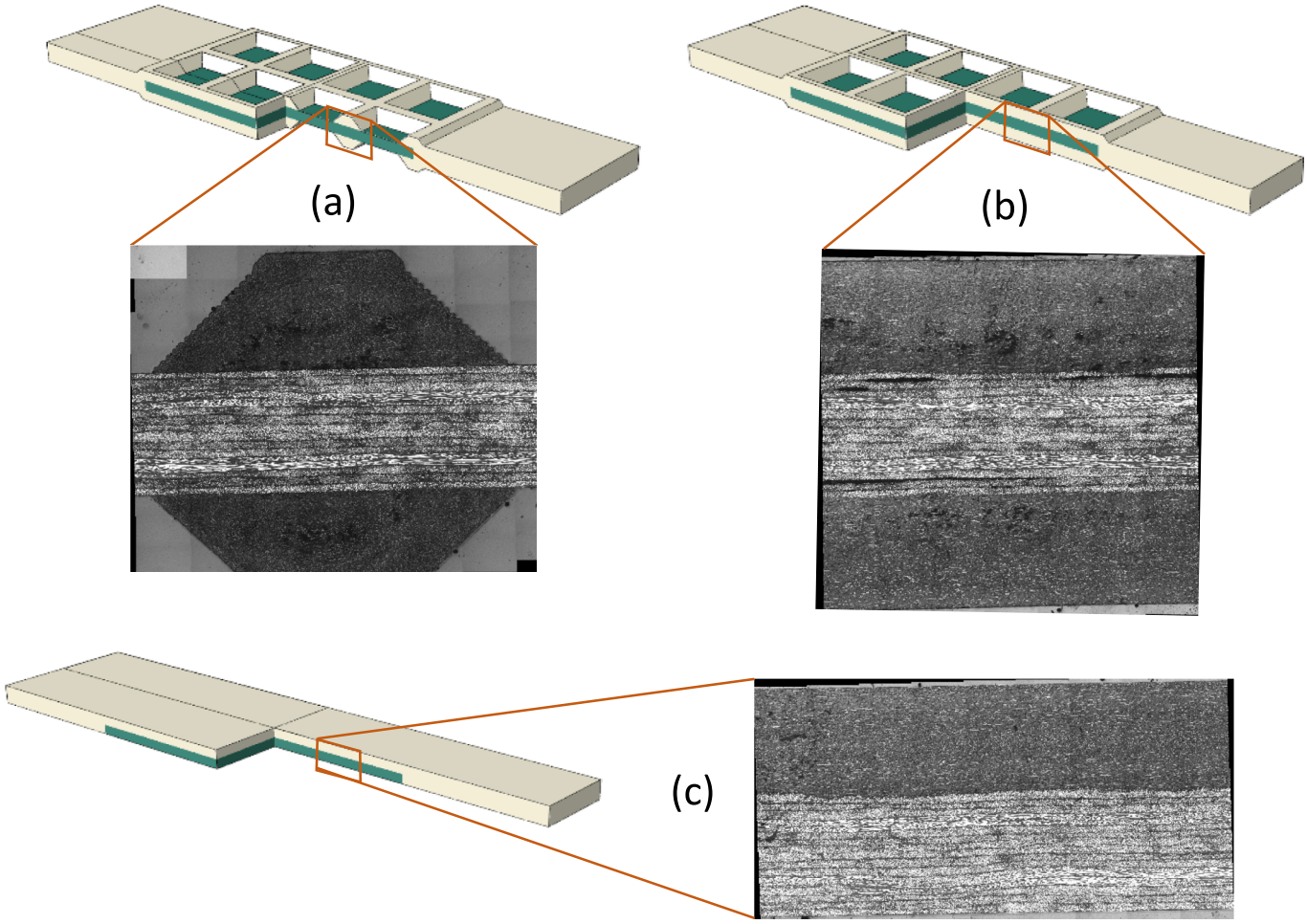

Fig. 16. Microscopy cross sections of rib areas in a Waffle specimen (a) and (b), showing areas of turbulent flow and cavitation, in comparison to cross section of Bias specimen (c).

overmoulding material. As can be seen in Fig. 10, there are considerable stress concentrations around the central rib, which will affect the performance of the interface.

Additionally, the assumption of a random in-plane fibre orientation for the overmoulding material is simplistic according to microscopy sections across the Waffle rib in Fig. 16. It is evident that the larger volume of the rib area experiences non-laminar flow, such that the assumed planar random fibre distribution (Krenchel factor of 0.375) is in fact closer to a fully 3D random fibre distribution in certain regions (Krenchel factor of 0.2). This is due to the unique fountain flow characteristics in these complex rib areas [24,25]. The models were run using Krenchel factors of both 0.375 and 0.2 for the Waffle configuration (see Fig. 15), however this alone does not account for the underperformance of the Waffle configuration at higher deflections (relative deflections > 0.25).

The microscopy sections in Fig. 16 also indicate a degree of cavitation, which is the likely result of shrinkage due to the inability to apply sufficient packing pressure to the trapped 'molten core' regions of the ribs during manufacturing. There also appears to be some delamination of the insert near to the surfaces, which may have occurred due to deconsolidation when the insert was placed inside the hot injection mould tool, or as a result of a 'wash' effect in proximity to the complex flow in the ribs. Both of these effects could contribute to micro-cracking and early onset of failure. Such issues can potentially be addressed by modifying the manufacturing conditions. For example, adjusting the melt fill rate would change the deflection forces that influence insert wash, as well as affecting fibre orientations and the layer thicknesses in the fountain flow region. Molten core issues could be mitigated by adjusting the cooling rate and packing pressure to ensure full solidification.

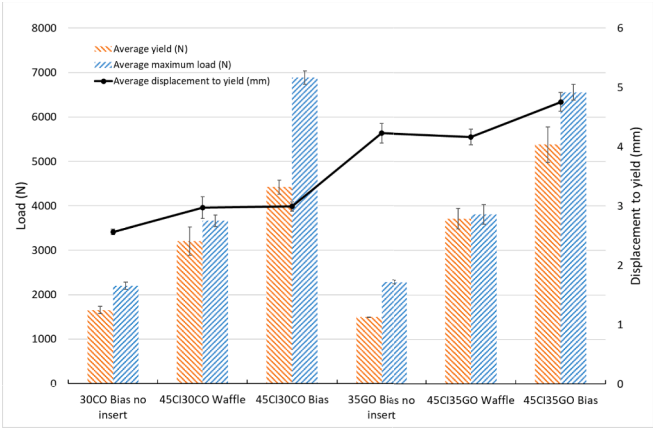

Fig. 17. Average experimental yield, maximum load and displacement to yield values for physical overmoulded specimens subjected to flexural (3 point bend) testing.

Yield and failure loads of the Waffle specimens are somewhat lower than for the Bias specimens, as can be seen in Fig. 17 (at about 70 % and 55 % respectively). The load at final failure is within 20 % of the load at

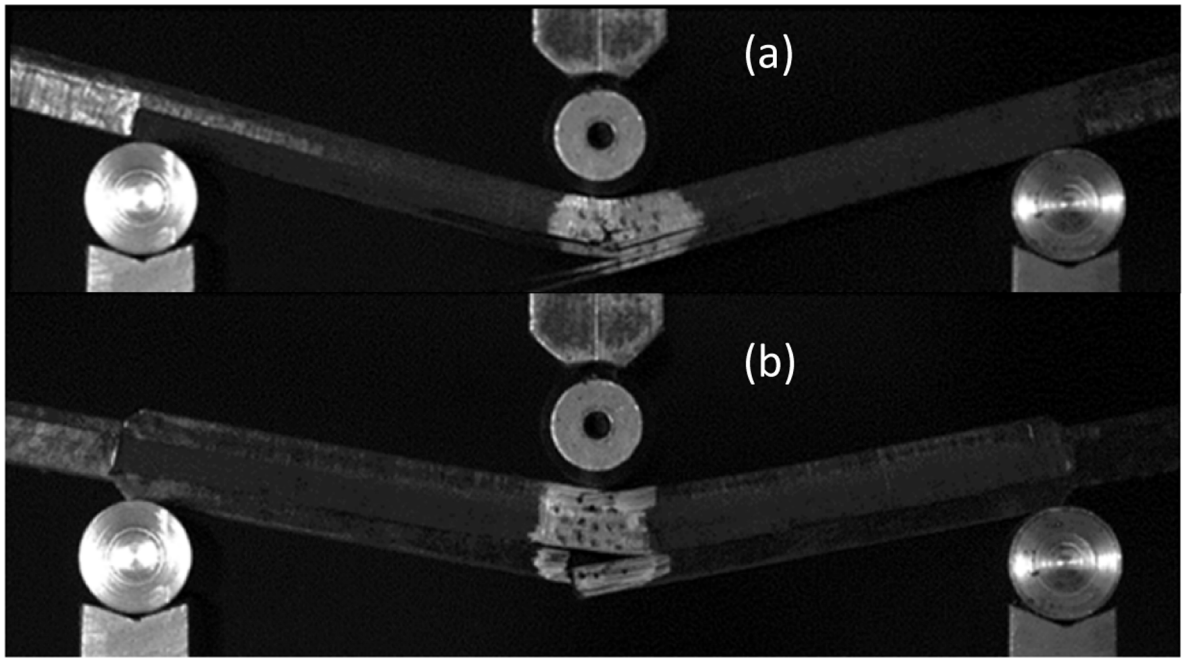

Fig. 18. Three point bending failure behaviour examples for 45CI35GO material in (a) Bias and (b) Waffle configurations.

yield for the Waffle samples, with a more prolonged failure after yield for the Bias samples.

The explanation for this prolonged failure, and perhaps for the underperformance of the Waffle against the model overall, lies in the difference in bending failure behaviour between the Waffle and Bias specimens. Whilst the Bias configuration fractures layer by layer through the laminate (Fig. 18a), the Waffle failure initiates through cracking of the outer layer of overmoulding material, with subsequent delamination failure between the overmould and the insert before final insert failure (Fig. 18b). This delamination failure demonstrates the relative significance of the interface for the Waffle geometry compared to the Bias samples. Performance will be highly dependent on the quality of the interface, lending this design perhaps to a 1-step overmoulding process that can achieve higher interfacial temperatures.

At the early stage of process design for manufacture, a simplified model is used to gain an initial understanding of this new process and to identify feasible solutions to rule out undesirable scenarios. In future studies, fibre orientation distributions will be captured through mould filling simulations or by physical methods such as microCT. Fill simulations can also potentially enhance the manufacturing cycle by identifying areas where molten core can occur, and determining conditions to minimise this effect. Combined with realistic interface properties this will provide a more robust simulation that can be expanded beyond the elastic region to capture more realistic predictions of failure, including those that are initiated at the interface between the insert and the overmoulding material.

4. Conclusions

Overall, this study has demonstrated that the application of a waffle-type structure to discreet insert moulding could provide significant benefits to component manufacturing; warp is avoided through symmetry of design, insert clamping is improved and part ejection is straightforward. Based on the model data, this could be achieved in theory with minimal impact on the primary stiffening role of the insert, with simulation indicating that the result could be superior with appropriate material pairings and manufacturing optimisation.

The application of Shear Lag theory provided a reasonable approximation for the transfer of shear stress between the insert and the overmoulding material at the interface, during tensile loading for the symmetrical configuration. However, this could not account for the non-zero strains at the insert ends. An alternative metric to gauge insert efficiency was proposed to aid material selection, which highlighted that a discrete insert would experience axial stress at only a small proportion of its failure limit, even with a perfect interface with the overmoulding material. Physical testing indicates that the Waffle structure reduces local strains in the transition zone between insert and overmoulding elements and increases the overall maximum tensile load to failure in comparison to the Bias case. However, there appears to be a significant dependency on the quality of the interface that causes underperformance against the model for both the Bias and Waffle cases.

In the bending tests, good agreement was seen between the model and the physical data for the Bias case, however the Waffle structure underperformed against the model. This may in part be due to fibre orientation and shrinkage issues, but is more likely due to a higher dependency on the quality of interface for the Waffle structure. Notably in the three point bend setup, the 50/50 split of overmoulding material and insert material means that the interface lies on the neutral axis in the Bias case but not in the Waffle case. The current form of the model does not account for interface failure and cannot provide a realistic appraisal of properties beyond the elastic region. Ultimately, it is expected that discrete insert moulding will remain a primarily stiffness driven design. With that in mind, surface plots were provided to indicate expected stiffness in bending for a wide range of pairings of insert and overmoulding modulus values.

CRediT authorship contribution statement

A.J. Parsons: Conceptualization, Data curation, Formal analysis, Funding acquisition, Investigation, Methodology, Validation, Visualization, Writing – original draft. **S. Chen:** Conceptualization, Data curation, Formal analysis, Investigation, Methodology, Software, Validation, Visualization, Writing – review & editing. **A. Ryder:** Conceptualization, Funding acquisition, Methodology, Resources, Writing – review & editing. **D. Bradley:** Conceptualization, Writing – review & editing. **N.A. Warrior:** Funding acquisition, Writing – review & editing. **L.T. Harper:** Conceptualization, Funding acquisition, Methodology, Project administration, Supervision, Writing – review & editing.

Declaration of competing interest

The authors declare that they have no known competing financial interests or personal relationships that could have appeared to influence the work reported in this paper.

Data availability

Data will be made available on request.

Acknowledgements

This work was funded by Innovate UK [Grant number: 40546] as part of the, "UK and USA: innovation in global composites market" Competition. The authors from the University of Nottingham also gratefully acknowledge financial support from the Engineering and Physical Science Research Council [Grant number: EP/P006701/1], through the "EPSRC Future Composites Manufacturing Research Hub".

References

[1] Schell JSU, Guilleminot J, Binetruy C, Krawczak P. Computational and experimental analysis of fusion bonding in thermoplastic composites: influence of process parameters. J Mater Process Technol 2009;209:5211–9.
[2] Kuehnert I, Pompsch I. Morphology and strength of injection molded parts with interfaces. Annual Technical Conference - ANTEC, Conference Proceedings2011. p. 1654-8.
[3] Behrens B-A, Dröder K, Brunotte K, Wester H, Hürkamp A, Ossowski T, et al. Numerical modelling of bond strength in overmoulded thermoplastic composites. J Compos Sci 2021;5:164.
[4] Akkerman R, Bouwman M, Wijskamp S. Analysis of the Thermoplastic Composite Overmolding Process: Interface Strength. Frontiers in Materials. 2020;7.
[5] Le Mouellic P, Boyard N, Bailleul J-L, Lefevre N, Gaudry T, Veille J-M. Development of an original overmoulding device to analyse heat transfer at polymer/polymer interface during overmoulding. Appl Therm Eng 2022;216:119042.
[6] Pisanu L, Santiago LC, Barbosa JDV, Beal VE, Nascimento MLF. Strength shear test for adhesive joints between dissimilar materials obtained by multicomponent injection. Int J Adhes Adhes 2018;86:22–8.
[7] Jiang B, Fu L, Zhang M, Weng C, Zhai Z. Effect of thermal gradient on interfacial behavior of hybrid fiber reinforced polypropylene composites fabricated by injection overmolding technique. Polym Compos 2020;41:4064–73.
[8] Hudacek L. How to optimize adhesion in hard-soft overmolding. plastics technology. Cincinnati, OH: Gardner Business Media Inc.; 2004. p. 63–8.
[9] Giusti R, Lucchetta G. Analysis of the welding strength in hybrid polypropylene composites as a function of the forming and overmolding parameters. Polym Eng Sci 2018;58:592–600.
[10] Valverde MA, Kupfer R, Wollmann T, Kawashita LF, Gude M, Hallett SR. Influence of component design on features and properties in thermoplastic overmoulded composites. Compos A Appl Sci Manuf 2020;132:105823.
[11] Tanaka K, Harada Y, Katayama T, Ishikawa T, Tomioka M. Press and injection hybrid molding using CF/PP unidirectional slit prepreg and evaluation of bonding strength at rib root. J Soc Mater Sci, Jpn 2016;65:721–6.
[12] Tanaka K, Kaetsu M, Katayama T, Ishikawa T. Effect of rib root shape on the tensile strength of press and injection hybrid molded products made with CF/PA6 random prepreg sheet. WIT Trans Built Environ 2018:93–100.
[13] Tanaka K, Karasuno K, Ryuichi N, Katayama T. Effects of press pressure on the mechanical properties of rib root for glass fiber reinforced polypropylene composites, molded by press and injection hybrid molding. WIT Trans Eng Sci 2017:317–26.
[14] Tanaka K, Noguchi R, Katayama T. Evaluation of mechanical properties of glass fiber reinforced polypropylene composites made by press and injection hybrid molding. J Soc Mater Sci, Jpn 2018;67:107–13.
[15] Tanaka K, Tokura D, Katayama T, Ishikawa T, Tomioka M. Evaluation of mechanical property of press and injection hybrid molded CF/PA6 using cut prepreg sheets. J Soc Mater Sci, Jpn 2016;65:713–20.
[16] Tanaka K, Yamada T, Katayama T. Evaluation of mechanical property of press and injection hybrid molded CF/PA6 using paper-type intermediate material. J Soc Mater Sci, Jpn 2018;67:114–20.
[17] Neveu F, Cornu C, Olivier P, Castanié B. Manufacturing and impact behaviour of aeronautic overmolded grid-stiffened thermoplastic carbon plates. Compos Struct 2022;284:115228.
[18] Häffelin D, Wagener K, Beutler O, Lutter F, Jecmeniza U. Lightweight design on the move. Kunststoffe International: Walter de Gruyter; 2017. p. 28-31.
[19] Ryder A. Enhanced Thermal Control of Mould Tooling as an Enabler for Thermoplastic. SAMPE Europe 2018. Southampton, UK2018.
[20] Aravand A. 13 - Composite injection overmoulding. In: Harper L, Clifford M, editors. Design and Manufacture of Structural Composites: Woodhead Publishing; 2023. p. 323-45.
[21] Harper LT, Turner TA, Warrior NA, Rudd CD. Characterisation of random carbon fibre composites from a directed fibre preforming process: the effect of tow filamentisation. Compos A Appl Sci Manuf 2007;38:755–70.
[22] Qiu YP, Weng GJ. On the application of Mori-Tanaka's theory involving transversely isotropic spheroidal inclusions. Int J Eng Sci 1990;28:1121–37.
[23] Jacquet E, Trivaudey F, Varchon D. Calculation of the transverse modulus of a unidirectional composite material and of the modulus of an aggregate. Application of the rule of mixtures. Compos Sci Technol 2000;60:345–50.
[24] Horst JJ, Spoormaker JL. Fatigue fracture mechanisms and fractography of short-glassfibre-reinforced polyamide 6. J Mater Sci 1997;32:3641–51.
[25] Tseng H-C, Chang R-Y, Hsu C-H. Predictions of fiber concentration in injection molding simulation of fiber-reinforced composites. J Thermoplast Compos Mater 2018;31:1529–44.
[26] Hull D, Clyne TW. An introduction to composite materials. 2 ed. Cambridge: Cambridge University Press; 1996.
[27] Cox HL. The elasticity and strength of paper and other fibrous materials. Br J Appl Phys 1952;3:72–9.
[28] Qian C, Harper LT, Turner TA, Warrior NA. Notched behaviour of discontinuous carbon fibre composites: comparison with quasi-isotropic non-crimp fabric. Compos A Appl Sci Manuf 2011;42:293–302.
[29] Fukuda H, Chou T-W. An advanced shear-lag model applicable to discontinuous fiber composites. J Compos Mater 1981;15:79–91.
[30] Galiotis C, Young RJ, Yeung PHJ, Batchelder DN. The study of model polydiacetylene/epoxy composites. J Mater Sci 1984;19:3640–8.
[31] Evans AD, Turner TA, Harper LT, Warrior NA. Design guidelines for hybrid continuous/discontinuous carbon fibre laminates. J Compos Mater 2022;56:1513–27.
[32] AZoM.com. E-Glass Fibre. 2001. https://www.azom.com/article.aspx?ArticleID=764, accessed July 2023.
[33] Krucinska I, Stypka T. Direct measurement of the axial poisson's ratio of single carbon fibres. Compos Sci Technol 1991;41:1–12.
[34] MatWeb. E-Glass Fiber, generic. 2022. https://www.matweb.com/, accessed July 2023.
[35] MatWeb. Overview of materials for Nylon 66, Unreinforced. 2022. https://www.matweb.com/, accessed July 2023.
[36] Minus M, Kumar S. The processing, properties, and structure of carbon fibers. JOM 2005;57:52–8.
[37] Toray. T300 Technical data sheet. Toray; 2018. https://www.toraycma.com/wp-content/uploads/T300-Technical-Data-Sheet-1.pdf.pdf, accessed July 2023.